Numerical and experimental investigations on cutting force of broaching internal spline holes

Shenshun Ying
Zhejiang University of Technology
Chentai Fu
Zhejiang University of Technology
Shunqi Zhang (sqzhangnpu@163.com)
Shanghai University https://orcid.org/0000-0003-0633-0564
Lvgao Lin
Zhejiang CHR Intelligent Equipment Co., Ltd

Research Article

Keywords: Cutting force, Johnson-Cook material model, force measurement, wavelet transform

Posted Date: June 18th, 2021

DOI: https://doi.org/10.21203/rs.3.rs-421007/v1

Version of Record: A version of this preprint was published at The International Journal of Advanced Manufacturing Technology on February 28th, 2022. See the published version at https://doi.org/10.1007/s00170-022-08739-7.

Numerical and experimental investigations on cutting force of broaching internal spline holes

Shenshun Ying[1], Chentai Fu[1], Shunqi Zhang[2,1], Lvgao Lin[3]

[1] Ministry of Education Key Laboratory of Special Purpose Equipment and Advanced Processing Technology, Zhejiang University of Technology, Hangzhou 310032, China,

[2] School of Mechatronic Engineering and Automation, Shanghai University, Shanghai 200444, China,

[3] Zhejiang CHR Intelligent Equipment Co., Ltd, Jinyun 321404, China

Abstract

Cutting force in broaching process is essential information for quality controlling, troubleshooting and tool life prediction, yet existing technical bottleneck in prediction and acquirement in internal spline holes broaching process. Based on the mechanics of orthogonal metal cutting, a numerical model of the cutting force in internal spline broaching is constructed by Johnson-Cook material constitutive and failure model taking friction on both rake face and flank face into consideration, and is used to numerically estimate the cutting forces. A measurement apparatus is developed and real-time cutting force is monitored, which contains the effects of structural vibration and can be divided into static cutting force and dynamic cutting force. Wavelet transform filtering method is therefore employed to separate the static component from dynamic component. Calculated value of the cutting force by numerical model is in good agreement with the static cutting force by experimental measuring. The model and measurement method are feasible in intelligent manufacturing where internal broaching process is used.

Keywords

Cutting force; Johnson-Cook material model; force measurement; wavelet transform;

1 Introduction

Parts of the spline hole are widely used for power transmission in automobile, railway and power engine, aircraft industries, as well as in robots, electronic equipment, instrument and apparatus, chemical mechanism. Broaching is the main approach to manufacture the complex internal and external profiles. One broaching process including roughing, semi-finishing, finishing operations usually achieves high surface integrity, geometric precision and processing productivity, which results in wide use in batch process spline of parts. In the design of fixtures, tools and machine tools for internal spline holes broaching process, cutting forces is the essential and necessary information been considered. Especially in the design of machine tools, they are the key indexes that determine the spindle power and the structural strength of the machine tool [1].

There are two kinds of approaches to explore the cutting force in broaching process, namely numerical simulation and experimental measurement. Regarding to the first approach, many researchers have proposed various models, such as empirical model[2,3], finite element calculation model[4-6] and orthogonal cutting model for the simulation of

* Corresponding author: Dr. Shun-Qi Zhang, at the School of Mechatronic Engineering and Automation, Shanghai University, P. R. China. Email: sqzhangnpu@163.com.

cutting force during the machining process. Sutherland et al.[7] developed mechanistic model for the cutting force system in the gear broaching process. Which is based on a description of the instantaneous chip load geometry and a relationship between the chip load and the three-dimensional cutting force system. Schroeter et al. [3] presented a method for calculation of the cutting forces with the Kienzle equation and the kinematics model of turn-broaching process. Schulze et al. [5] studied the influence of variable cutting thickness and variable rake angle on cutting force through two-dimensional (2D) cutting simulations. By introducing a material constitutive model, Tounsi et al. [8] derived the expressions of effective stress, strain, strain rate and temperature on the main shear plane, and established a new orthogonal cutting mechanical model. Hosseini[9] presented a cutting forces model with the cutting edge assumed as a B-spline parametric curve for computation of the cutting forces for orthogonal and oblique broaching. Ni[10] analyzed the influences of the circular arc effect on the cutting force during the machining of the key hole of the inner hole considering the geometric and kinematic characteristics of the broaching, and proposed a cutting force model for the inner hole.

The efforts performed in the literature so far have focused on surface broaching that widely used in manufacture fir tree or dove tail slots for turbine disc process, while few literatures are reported about cutting force modelling for internal spline hole broaching[1,11,12]. Because the broaches used in internal spline holes process has the characteristics of cylindrical geometry, which causing a radial cancellation of cutting forces. In addition, due to multiple tooth on the circumference of the spline broach, a lot of heat is generated in the cutting process, which makes the temperature of the workpiece rise and causes the friction between the expansion of the workpiece and the flank face. However, cutting force models of broaching process in the literature so far have focused on the rake face and the workpiece, ignoring the friction force between the flank face and the processed surface of the workpiece during the broaching process.

Experimental measurements are direct means to obtain cutting force data in broaching process, and are usually used to prove the calculation results of the numerical simulation, as well as the online monitoring for broaching state. Klocke et al.[13] specially designed a piezoelectric 3-component dynamometer for broaching machine tool, and integrated the force measurement system as a part of the machine between the machine and the indexing table. Many scholars adopted a three-component Kislter dynamometer to monitor the three-dimensional cutting force signal of the broaching machine[14,15]. However, the dynamometer is installed on the face table of the broaching machine, which requires customization and high cost. Moreover, because the broach runs through the table in internal spline broaching process, it is difficult to measure the cutting force using Kislter platform dynamometer or an integrated version, relevant research results are rare and it should be strengthened further.

This paper presents a cutting force model for the internal spline broaching, by taking the friction on both rake face and flank face into consideration. A cutting force measurement apparatus is developed, which especially suitable for internal hole broaching, and Wavelet transform filtering method is additionally employed to reduce unnecessary dynamic response. In addition to the part of introduction, this paper is organized as follows. Based on the orthogonal cutting mechanical model, a numerical model of internal spline cutting force is firstly established by introducing the friction factor of flank face. Subsequently, a dexterous measurement apparatus for cutting force in broaching operation was designed, and the influence of the dynamic force caused by the broaching tool entering and emerging the workpiece was considered. The wavelet transform was used to eliminate the dynamic distortion and achieve accurate

measurement of cutting force, then the model was tested and verified. At last the conclusion of this paper is pointed out.

2 Modelling of cutting force in broaching internal spline holes

2.1 The geometric characteristics of internal spline holes broaching

Broaching is a material removal process using a multiple-edged tool whose cutting edges are arranged in a line and with a "rise per tooth" (RPT)), which determines the depth of cut per tooth. The tool is moved in one direction only; the feed and width of cut are hereby determined by the tool geometry. The size and shape of the final teeth correspond to the desired geometry of the workpiece. After one single pass of the tool through the workpiece, namely, a broaching stroke, the process is complete, and the workpiece's surface is finished at the same time. In general, the translational motion is run by the tool at a stationary workpiece[16].

Internal broaching is characterized by symmetrical geometries in inner diameters. The broaching tool is thereby pulled or pushed through the workpiece, shown in Fig.1. Through-holes and a sufficient minimum wall thickness to prevent deflection due to the radial cutting forces are preconditions for internal broaching[17].

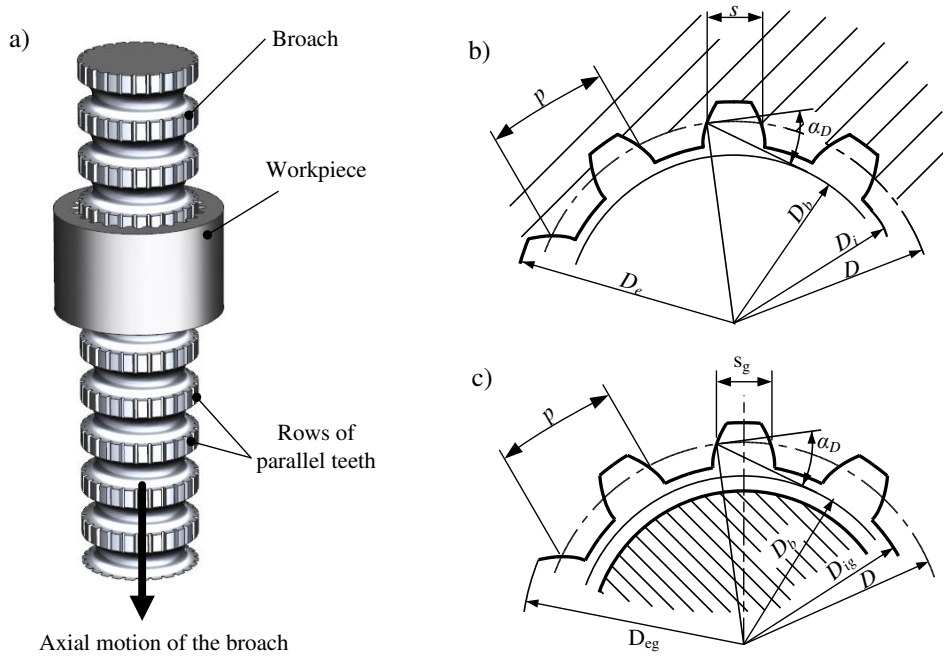

(a) Internal spline hole broaching process geometry and kinematics; (b) Work involute spline; (c) Broach tooth shape of involute internal spline (finish section)

Fig.1. Internal spline holes broaching process geometry and kinematics

Table.1. Broach tooth and work involute spline geometry

Circumferential tooth pitch	p
Standard pressure Angle	α_D
tooth thickness	s
Involute dividing circle diameter	D
Minor diameter	D_i
Base diameter	D_b
Major diameter	D_e
Note: the subscript g is the broach size	

2.2 Orthogonal cutting theory and Johnson-Cook material model

Broaching is essentially a kind of orthogonal cutting. Tounsi et al.[8] theoretically derived the expressions of the effective stress, strain, strain rate and temperature on the main shear plane caused by the stress, strain, strain rate and temperature fields, and proposed the basic mechanics of the main shear zone in the orthogonal cutting. During the cutting process, the friction between the tool and the workpiece mainly occurs on the rake face. The force model of the workpiece is obtained through the balance of forces, as shown in Fig. 2(a).

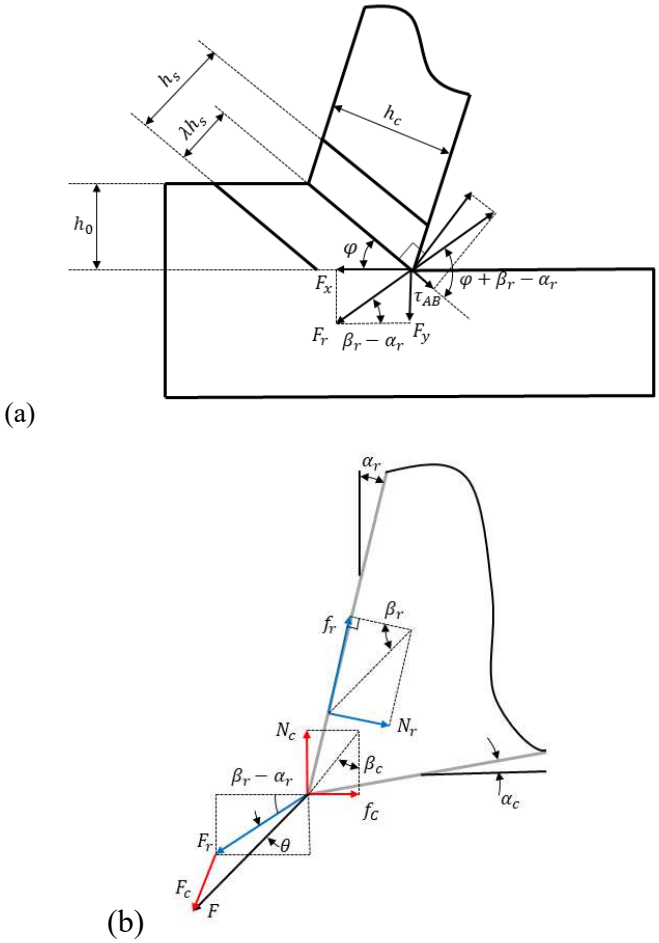

Fig. 2. Orthogonal cutting model: (a) Workpiece force model; (b) Tool force model

On this basis, considering that the workpiece generates heat during the cutting process, the temperature of the workpiece increases, causing the workpiece to expand and friction with the flank face. The cutting force is mainly composed of shear force and friction force of flank surface, as shown in Fig. 2(b). The vector method of the resultant cutting force is expressed as:

$$F = F_r + F_c \tag{1}$$

where F_c is the friction force between the flank face and the workpiece due to thermal expansion deformation, F_r is the shear force.

The components of the resultant cutting force along the X and Y axes respectively are the main cutting force and the radial thrust force, Shown in Fig. 2

$$F_X = F_r \cos(\beta_r - \alpha_r) + f_c \tag{2}$$

$$F_Y = F_r \cos(\beta_r - \alpha_r) + N_c \tag{3}$$

where f_c is the friction force of the flank face, N_c is the support reaction of the flank face. According to orthogonal cutting theory, the shearing force of single tooth can be expressed as:

$$F_r = \frac{\tau_s W_i h_i}{\sin\varphi\cos(\varphi+\beta_r-\alpha_r)} \tag{4}$$

Where β_r is the friction angle of tooth, α_r is the rake angle of tooth, τ_s is shear stress, W_i is cutting width, h_i is rise per tooth, and φ is shear angle.

Base on Johnson-Cook material and failure model, the shear stress τ_s on the shear plane is given by [8]:

$$\tau_s = \frac{1}{\sqrt{3}}(A+B\gamma^{n_s})\left(1+C\ln\frac{\dot{\gamma}}{\dot{\gamma}_0}\right)\left(1-\left(\frac{T-T_0}{T_m-T_0}\right)^{m_s}\right) \tag{5}$$

where A is yield strength, B is hardening modulus, C is strain rate, n_s is strain hardening index, m_s is material heat sensitive parameters, γ is the shear strain, $\dot{\gamma}$ is the shear strain rate, $\dot{\gamma}_0$ is the reference shear strain rate, T is the cutting temperature of the workpiece, T_0 is initial temperature, and T_m material melting temperature. The cutting temperature on the main shear surface is expressed as:

$$T = T_0 + \left[\frac{\lambda\cos\alpha_r}{\rho C_p\sin\varphi\cos(\varphi-\alpha_r)}\right]\left(\frac{2\tau_s+\tau_0}{3}\right) \tag{6}$$

where ρ is mass density, C_p is specific heat, τ_0 is shear stress at main shear zone inlet.

The shear angle generally needs to be obtained through experimental measurement, and can also be approximated according to the coefficient of expansion of the chip after material cutting:

$$\Lambda = \frac{h_c}{h_i} = \frac{\cos(\varphi-\alpha_r)}{\sin(\varphi)} \tag{7}$$

where h_c is chip thickness. It can be measured according to the actual chip or according to the material properties. Based on[18], the friction angle β_r can be calculated by:

$$\beta_r = \frac{\pi}{2}+\alpha_r-2\varphi \tag{8}$$

The γ and $\dot{\gamma}$ can be calculated by:

$$\begin{cases}\gamma = \dfrac{\lambda\cos(2\alpha_r)}{\sqrt{3}\cos(\varphi-\alpha_r)\sin(\varphi)} \\ \dot{\gamma} = \dfrac{2V\cos(\alpha_r)}{\sqrt{3}h_s\cos(\varphi-\alpha_r)}\end{cases} \tag{9}$$

where λ is the main shear zone coefficient.

$$\lambda = \frac{1}{2}+\frac{\cos(2\varphi-\alpha_r)}{2\cos(\alpha_r)} \tag{10}$$

The friction force and support reaction of the rear surface can be expressed as:

$$f_c = \mu N_c \tag{11}$$

$$N_c = 0.5YK_E\Delta TWL_c \tag{12}$$

Where μ is friction coefficient, Y is young modulus of workpiece, K_E is workpiece

material thermal expansion coefficient, ΔT is temperature difference between workpiece cutting and initial state, L_c is contact length of the workpiece with the flank surface after expansion. The formula for estimating the contact length L_c is given by

$$L_c = \frac{K_E \Delta T h_T}{2 \sin \alpha_c} \tag{13}$$

where h_T is temperature transfer depth, α_c is tool clearance angle.

By using Newton's nonlinear solution method and solving equations (5) and (6) simultaneously, the real-time stress can be obtained.

2.3 Effect of teeth number engaged in broaching on the cutting force

In the broaching process of involute spline holes parts, the number of teeth involved in cutting varies because the teeth are distributed in row by row. The broaching process is mainly divided into three stages. The first stage is when the cutter teeth enter the workpiece, and the number of teeth increases at the initial contact stage until the maximum number of teeth in contact. In the second stage, the cutter teeth are in full contact with the workpiece, and the contact teeth are periodic until the workpiece begins to leave the cutter teeth. The third stage is the stage when the cutter teeth exit the workpiece, and the number of contact teeth decreases until the cutter teeth completely leave the workpiece. The basic formula of multi-tooth cutting force modeling is given in Ref. [10]. The change formula of the number of broaching teeth during broaching can be expressed as:

$$i = \begin{cases} n & 0 < t < \dfrac{Z_{\max} p_a}{v_c} \text{ and } n <= Z_{\max} \\ Z_{\max} & \dfrac{(n-1)\cdot p_a}{v_c} \le t < \dfrac{L + (n - Z_{\max})\cdot p_a}{v_c} \\ Z_{\max} - 1 & \dfrac{L + (n - Z_{\max})\cdot p_a}{v_c} \le t \le \dfrac{n p_a}{v_c} \end{cases} \tag{14}$$

$Z_{\max} = [L / p_a]$; $[\cdot]$ is ceiling function.

Based on the above analysis, the mechanical modeling of multi-tooth broaching can be described as:

$$F_{total} = \begin{cases} \sum_{0}^{i} F_i & 0 < t < \dfrac{Z_{\max} p_a}{v_c} \\ \sum_{n-i}^{n} F_i & \dfrac{Z_{\max} p_a}{v_c} \le t < \dfrac{(Z - Z_{\max}) p_a}{v_c} \\ \sum_{i}^{Z} F_i & \dfrac{(Z - Z_{\max}) p_a}{v_c} \le t \le \dfrac{Z p_a}{v_c} \end{cases} \tag{15}$$

where n is number of teeth into broaching, Z is total number of teeth of broach, L is workpiece height, p_a is axial tooth pitch.

2.4 Cutting simulation of an internal spline hole broaching

Based on the above model, the cutting force simulation of involute spline broaching was carried out. The geometric and material parameters of the workpiece and broaching tool were shown in Table.2.

Table.2. Input parameters for numerical and analytical models

Material (Q235A steel) properties				
Johnson-Cook	constitutive	A	(MPa)	293.8

parameters[19]	B	543
	C	0.045
	n_s	0.489
	m_s	0.942
Mass density	ρ (kg/m^3)	7870
Main shear zone coefficient	λ (W·m^{-1}·K^{-1})	51.9
Initial strain rate	$\dot{\gamma}_0$ (s^{-1})	0.021
Specific heat	C_p (J·kg^{-1}·K^{-1})	469
Initial temperature	T_0 (K)	298.15
Melting point	T_m (K)	1795
Young modulus	Y (GPa)	200
Linear expansion coefficient	K_E (K^{-1})	11.2×10^{-6}
Contact		
Coefficient of friction （Contact properties）	μ	0.3
Coefficient of expansion	Λ	2.2
Tool parameters		
Rake angle	α_r (°)	15
Clearance angle	α_c (°)	7
Axial tooth pitch	p_a (mm)	13
Number of teeth per row		8
Number of teeth row		46
Rise per tooth" (RPT)	h_i (mm)	Refers to Table.3
Cutting width	W_i (mm)	
Tooth bottom width	w (mm)	
Work geometry and process conditions		
Minor diameter	D_i (mm)	46/65
Standard pressure Angle	α_D (°)	
Workpiece height	L (mm)	40
Cutting speed	v (mm/s)	0.045

The parameters of cutting width calculation refers to Fig.3.

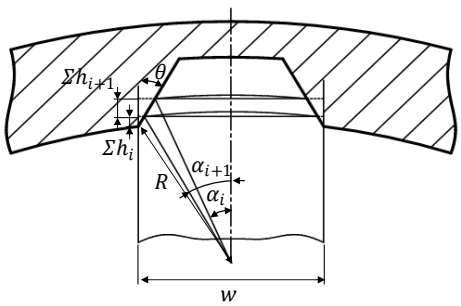

Fig.3. Cutting width calculation for internal spline hole broaching

where $\sum h_i$ is the sum of cutting depth before the i^{th} tooth, D_i is the initial part inner radius, shown in Fig.1. α_D is the tilt angle, approaching to pressure angle of work

spline, shown in Fig.1. w is the tooth bottom width.

$$\alpha_i = \arctan\left(\frac{0.5b - \tan\alpha_D \sum h_i}{\sqrt{D_i^2 - w^2} + \sum h_i}\right) \quad (16)$$

$$W_i = 2\alpha_i \frac{0.5b - \tan\alpha_D \sum h_i}{\sin\left(\frac{180\alpha_i}{\pi}\right)} \quad (17)$$

The calculation result is show in Table. 3.

Table.3. Cutting depth and cutting width

i	h_i	W_i	i	h_i	W_i
1	0.02	130.12	24	0.05	46.05
2	0.03	130.20	25	0.08	44.93
3	0.02	130.26	26	0.06	44.37
4	0.03	130.37	27	0.04	44.00
5	0.02	130.43	28	0.08	43.26
6	0.02	130.49	29	0.03	42.98
7	0.01	130.57	30	0.08	42.05
8	0.04	53.79	31	0.03	41.58
9	0.05	53.51	32	0.1	40.65
10	0.05	53.33	33	0.06	40.09
11	0.06	52.76	34	0.05	39.63
12	0.03	52.11	35	0.04	39.26
13	0.08	51.74	36	0.1	38.33
14	0.04	50.99	37	0.08	37.59
15	0.05	50.52	38	0.05	37.12
16	0.03	50.24	39	0.09	36.29
17	0.07	49.59	40	0.1	35.36
18	0.06	49.03	41	0.05	34.90
19	0.04	48.66	42	0.06	34.34
20	0.06	48.10	43	0.06	33.78
21	0.05	47.63	44	0.06	33.23
22	0.03	47.35	45	0.07	32.58
23	0.07	46.70	46	0.06	32.02

Under above mentioned broaching conditions, the cutting force calculated using the numerical model proposed in this paper is shown in Fig.4.

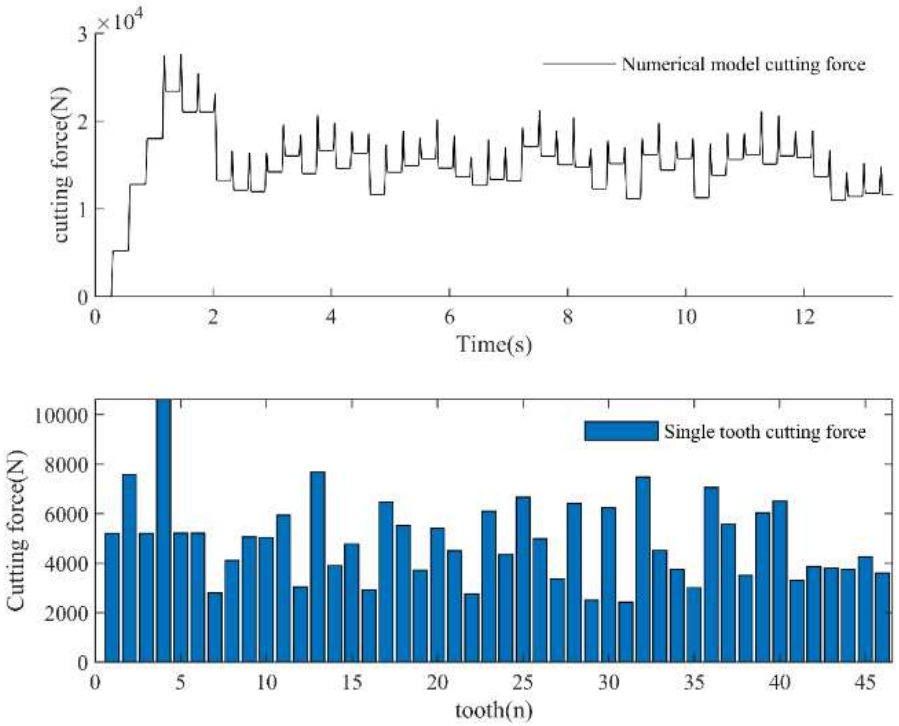

Fig.4. Numerical results of cutting force

3 Force measuring and processing for internal spline holes broaching

3.1 Force signal measurement method

For inner hole broaching, it is difficult to use commercial assembly dynamometer because the broach passes through the face table. In this paper, a simple device is designed to measure the broaching force of the inner hole by using strain gauge.

(1) Design of measuring apparatus

Fig.5 shows the force measurement system. A force measuring support plate is made on the broaching machine face table, the workpiece is placed on the force measuring support plate, the support and the face table are connected by four force measuring support columns, and the columns, support plate and face table are all connected by screws. The PCB strain sensor is pasted on the surface of the column, and the main strain direction of the strain sensor is along the longitudinal centerline of the column, so it is also pasted along the longitudinal centerline. All electrical signals are coupled with LMS SCADAS III 24-channel data acquisition system. LMS Test.lab software running on a computer workstation(DELL M90) controls the data acquisition and the analysis on all measured signals.

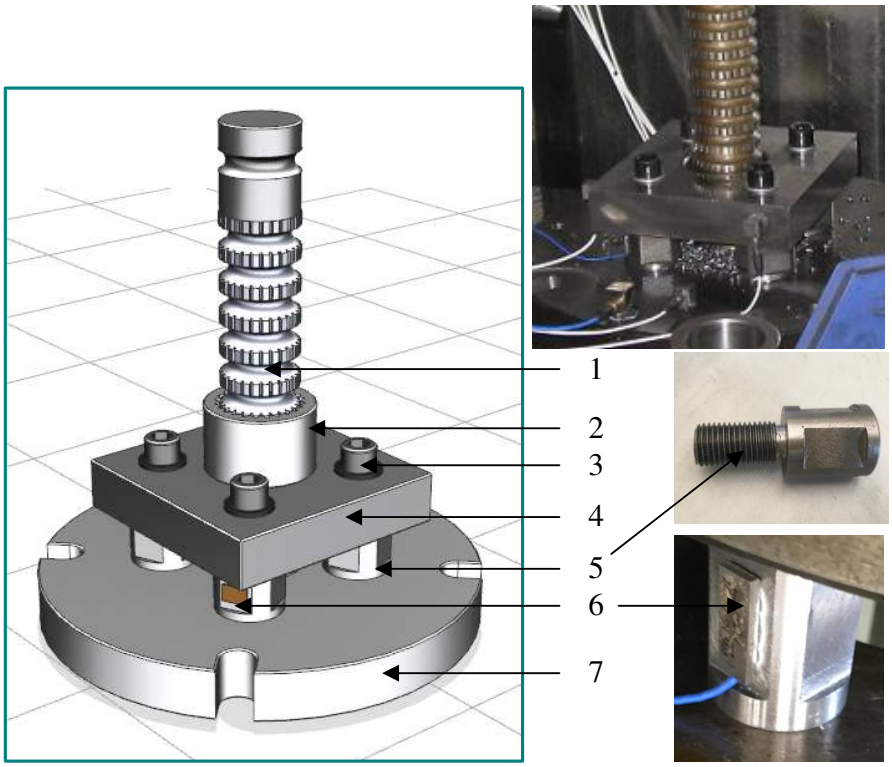

Fig.5. Force measuring mechanism for internal spline holes broaching

Description of components in experimental setup

Part #	Description
1	Broaching tool
2	workpiece
3	Screw
4	Force measuring support plate
5	Force measuring support column
6	Strain gauge
7	Broaching machine face table

(2) Sensitivity calculation

The strain gauges are attached to the force support columns, and the test sensitivity is calculated as follow

$$S = \frac{S_0 F}{E S_c} \tag{18}$$

where S_0 is strain sensor sensitivity, F is the cutting force, E is the Young's modulus of the support columns material, S_c is the cross-sectional area.

The designed column diameter is 40 mm, and the cross-sectional area after cutting is 81.12% of the original area. Assuming that the strain sensor is subjected to a force of 10 KN and the sensitivity of the strain sensor sensitivity is 50 mv/N, the test sensitivity is $0.2337 mv/N$. Since there are four support columns are used, each column is subjected to 1/4 cutting force, one can deduced the sensitivity of the strain gauge on each column should be set to $0.0584\, mv/N$.

3.2 Force signal decomposition based on wavelet transform

The number of cutter teeth and the RPT engaging in cutting process are changing, which results in a varying cutting force during the broaching process. The varying cutting force is composed of two parts: static cutting force and dynamic cutting force, of which the static cutting force component corresponds to a constant main cutting force,

the dynamic force component corresponds to the dynamic cutting force of the cutter teeth in and out of the workpiece, in addition to the impact of structural vibration. The decomposition purpose of the cutting force signal is to separate the dynamic and static components in the signal to extract the main cutting force. Fourier transform, bandpass filtering and wavelet packet decomposition can all be used for force signal decomposition[20]. Compared with the other two decomposition technologies, wavelet transform has the capability of multi-resolution, representing local features in both time and frequency domains, and multi-scale refinement of signals by scaling and translation.

(1) Wavelet transform theory

According to the discussion of the wavelet transform in literatures[21,22], $\psi(\mathrm{t})$ is in the Hilbert space $L^2(R)$ norm and satisfies the following admissible conditions $\int_R \psi(\mathrm{t})dt = 0$, then $\psi(\mathrm{t})$ is the mother wavelet. After the mother wavelet is scaling and shifting, a wavelet sequence can be expressed as:

$$\psi_{a,b}(t) = |a|^{-1/2}\, \psi(\frac{x-b}{a}) \tag{19}$$

where a is the scaled factor and b is the translation factor. The factor $|a|^{-1/2}$ is used to ensure energy preservation.

The continuous wavelet transform (CWT) of the signal $f(t)$ is defined as:

$$CWT_{a,b} = |a|^{-1/2} \int_{-\infty}^{+\infty} f(t)\, \overline{\psi \frac{x-b}{a}} dt \tag{20}$$

where $\overline{\psi_{a,b}}$ is the complex conjugate of $\psi_{a,b}$ generated by scaling and shifting.

A set of scaled and translated wavelet sequences can be generated by changing the parameters a and b, so the time scale characteristics of the signal $f(t)$ can be analyzed by the inner product of the scaled and translated wavelet sequences. Since the translation factor and the scaling factor of continuous wavelet transform are real numbers of continuous transform, continuous integration is inconvenient when processing digital signals. In order to obtain the numerical result of wavelet transform, the discrete wavelet transform (DWT) can be obtained by discretizing the scaling factor a and translation factor b. Discrete wavelet transform normally is conducted by dyadic discretization, the scale factor a and the translation factor b are discretized as follows:

$$a = 2^m, b = k2^m \quad k, m = Z \tag{21}$$

Combined with Eq. (21), Eq. (20) can be transformed into

$$\psi_{m,k}(t) = 2^{-m/2}\psi(\frac{x-k2^m}{2^m}) = 2^{-m/2}\psi(2^{-m}x - k) \tag{22}$$

The discrete wavelet transform is defined as

$$DWT_{a,b} == \int_{-\infty}^{+\infty} f(t)\overline{\psi_{m,k}(t)}dt \tag{23}$$

(2) Force decomposition process

In the wavelet decomposition process, the low-frequency coefficients are decomposed into two parts, namely, a new low-frequency coefficient vector and a high-frequency coefficient vector. The information lost between two consecutive low-frequency vectors is obtained by the high-frequency coefficient vector. Then, the new low-frequency coefficient vector continues to be decomposed into two parts, while the high-frequency coefficient vector will not be decomposed again. At the specified scale, the signal can be further written as

$$f(t) = A_J(t) + \sum_{j \le J} D_j(t) \tag{24}$$

where $D_j(t)$ is the detail parameter of signal $f(t)$ on scale J, and $A_J(t)$ is the approximate parameter of signal $f(t)$ on scale J.

Above process forms a decomposition tree as shown in Fig.6, which decomposes the signal into a number of detailed signals and one approximated signal. In broaching process case, the approximated signal captures the low frequency components corresponding to the static components of the cutting force signal, and the detailed one reflects the high frequencies corresponding to the dynamic components of the signal, taking the Weight into consideration.

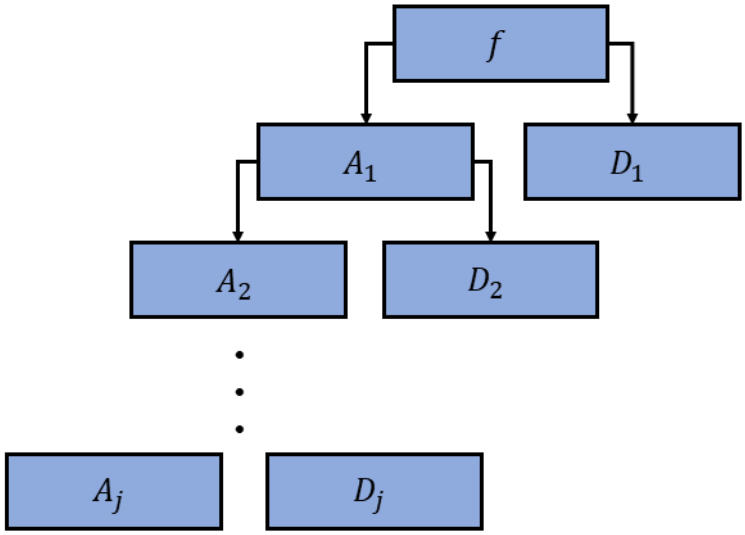

Fig.6 Wavelet transform decomposition tree

3.3 Experiment measuring and processing example

The physical force measuring apparatus, as well as the experimental platform, basing on a 15120SH-1200 broaching machine, are shown in Fig.5. The maximum process force of the broaching machine is 200 KN, the broaching stroke is 1200 mm, and the maximum broaching speed is 8 $m/\min$. The geometrical sizes and material coefficient of workpiece, as well as the tool parameters, are shown in Table.2.

The LMS SCADAS III data acquisition system is connected to a strain sensor to measure the cutting force, and the sampling results are recorded through the LMS Test.Lab software. The test equipment and performance parameters are shown in Table.4.

Table.4. Test apparatus and performance parameters

	apparatus	performance
PC	Dell /M90	
Data acquisition	LMS SCADAS III	24-channel Maximum sampling frequency/204.8kHZ
Software	LMS Test.Lab	
Strain sensor	PCB740B02	Sensitivity (±20%) 50 mV/με Range 100 pk με Bandwidth resolution 0.6με Frequency Range 0.5 to 100 000 Hz

In this experiment, a spline broaching processing is conducted, and the broaching speed is set to $0.045m/s$. The cutting force signal obtained by the force measurement

method proposed in this paper is shown in Fig.7.

A series of experiments have been completed using the force measurement system, and each group of experiments has good repeatability. This paper randomly extracts a group of test data for explanation. The curve in Fig. 8 describes the changes in cutting force during the reaming and roughing stages during the internal splines broaching. In the initial stage of contact between the workpiece and the broach, the cutting force gradually increases. In the stage of full contact between the broach and the workpiece, the number of broaching teeth is maintained at 3-4. The dynamic cutting force is generated when the cut edges of broach enter and leave the workpiece. The cutting force changes alternately with peaks and troughs. In Fig.7, the maximum cutting force measured by the experiment is 37120 N, however, the maximum cutting force of the numerical model is 27540 N, presented in Fig.4. It can be clearly seen that there is a large deviation between the cutting force of the numerical model and the measured cutting force.

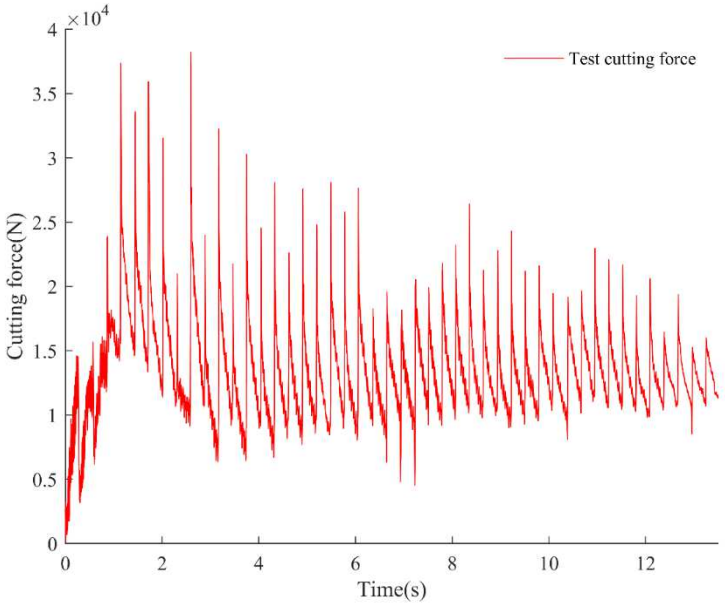

Fig.7 Cutting force test results

The measured cutting force is essentially affected by the dynamic force generated by the tool entering and leaving the workpiece, and cannot provide the characteristics of the actual cutting force in the broaching process. In order to obtain the actual cutting force acting on the tool/workpiece, the measured cutting force is decomposed using the method described in Section 3. The central frequency and bandwidth of the wavelet-based cascade filter depends on the choice of scale. "db5" is selected as the mother wave from the family of Daubechies wavelet due to its closest to the original data curve characteristics and performance in terms of time-frequency resolution, and correspondingly the decomposition scale is always specified as $J=8$ throughout. As a result, the test cutting force is divided into static cutting force and dynamic cutting force, as shown in Fig. 8. It can be seen that the amplitude of curve has dropped significantly.

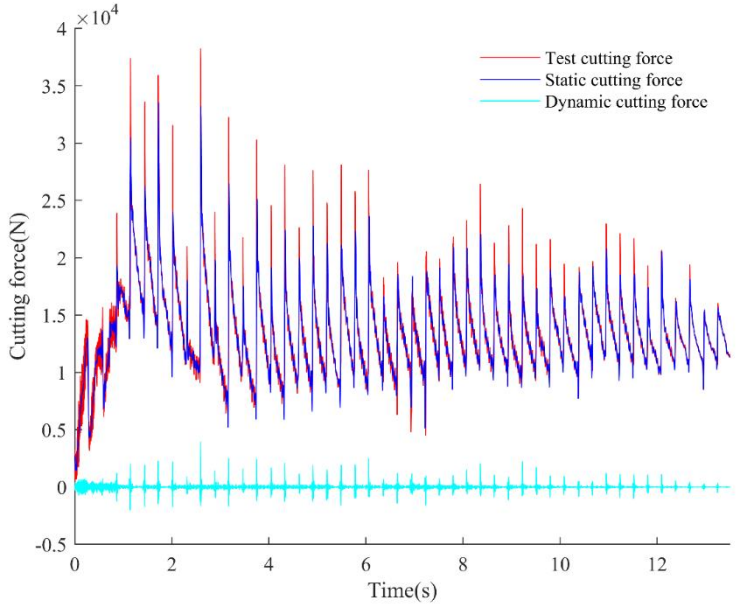

Fig.8 Cutting force decomposition results

4 Results analysis of numerical simulation and experimental measuring

Fig.9 shows the comparison between the decomposed static cutting force and the numerical model cutting force. In the figure, the maximum static cutting force is 28560N, and the maximum cutting force of the numerical model is 27540 N. Both the static cutting force and the numerical model cutting force curve show a trend of increasing first and then decreasing to a stable trend, and the peaks and troughs alternately change. The numerical model cutting force peak and static cutting force peak reached a good consistency. Compared with the static cutting force results, the numerical model results can better describe the broaching process. At the end of the reaming phase, the maximum error exceeds 30%. The remaining stages are less than 16%.

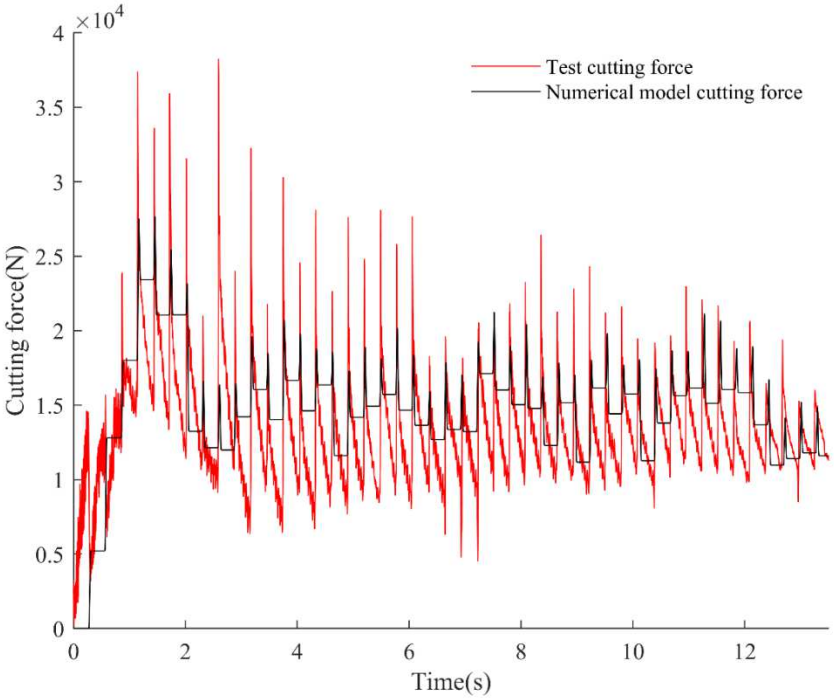

Fig.9 Test cutting force and Numerical model cutting force

The peak value of the numerical model is not completely fitted with the static cutting force, which is mainly affected by the complexity of the movement of the broaching drive components and the machining accuracy of the cutter tooth lift. However, it can be seen from Fig.10 that the cutting force numerical model established in this paper can effectively improve the calculation accuracy of broaching load.

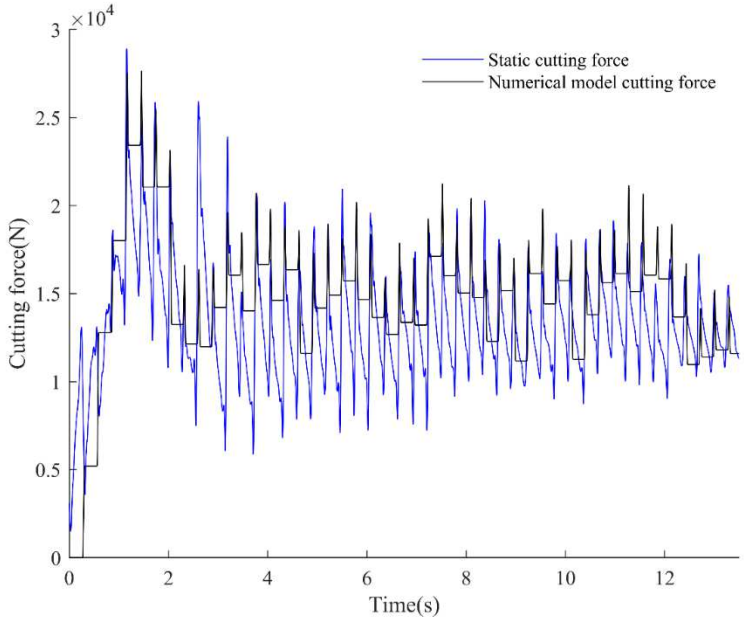

Fig.10 Static cutting force and Numerical model cutting force

5 Conclusions

This paper focuses on numerical modeling and accurate measurement of cutting force of inner spline hole in broaching process. The orthogonal cutting based numerical model of broaching force takes friction on both rake face and flank face into consideration, that especially reflects the symmetrical geometries and mechanics characters in inner broaching process. On the other hand, the force measurement apparatus is designed for actual working conditions, where the broaching tool passes through the face table. Wavelet transform decomposition is employed on the measured force signals to separate the dynamic force component, which eliminate the impact of the cutter teeth entering and leaving of the workpiece, as well as the structural vibration during the machining process. The results of numerical simulation were compared and shown in good agreements with those obtained by experimental measurement and Wavelet dynamic, and demonstrates the validity of the presented numerical model and measurement apparatus for cutting force in broaching internal spline holes.

Funding This work was supported by National Natural Science Foundation of China (Grant No. 11972020) and Natural Science Foundation of Zhejiang Province (Grant No. GG21E050049).

Author contributions All the authors have contributed equally for the paper.

Availability of data and material All data and material used to support the findings of this study are included within the article.

Compliance with ethical standards

Ethical Approval The article follows the guidelines of the Committee on Publication Ethics (COPE) and involves no studies on human or animal subjects.

Consent to participate The authors consent to participate.

Consent to publish Informed consent was obtained from all individual participants involved in the study.

Competing interests The authors declare that they have no conflicts of interest.

References

[1] Ortiz-De-Zarate G, Sela A, Saezdeburuaga M et al (2019) Methodology to establish a hybrid model for prediction of cutting forces and chip thickness in orthogonal cutting condition close to broaching. INT J ADV MANUF TECH 101(5): 1357-1374.

[2] Goncalves D, Schroeter R B (2016) Modeling and simulation of the geometry and forces associated with the helical broaching process. INT J ADV MANUF TECH 83: 205-215.

[3] Schroeter R B, Bastos C M, Filho J M C (2007) Simulation of the main cutting force in Crankshaft turn broaching. INT J MACH TOOL MANU 47(12-13): 1884-1892.

[4] Mabrouki T, Courbon C, Fabre D et al (2017) Influence of Microstructure on Chip Formation when Broaching Ferritic-Pearlitic Steels. Procedia CIRP 43-48.

[5] Schulze V, Boev N, Zanger F (2012) Numerical Investigation of the Changing Cutting Force Caused by the Effects of Process Machine Interaction While Broaching. 3rd CIRP Conference on Process Machine Interactions (3rd PMI) 140-145.

[6] Vogtel P, Klocke F, Puls H et al (2013) Modelling of process forces in broaching Inconel 718. 14th CIRP Conference on Modeling of Machining Operations (CIRP CMMO) 404-414.

[7] Sutherland J W, Salisbury E J, Hoge F W (1997) A model for the cutting force system in the gear broaching process. INT J MACH TOOL MANU 37(10): 1409-1421.

[8] Tounsi N, Vincenti J, Otho A et al (2002) From the basic mechanics of orthogonal metal cutting toward the identification of the constitutive equation. INT J MACH TOOL MANU (42): 1373-1383.

[9] Hosseini A, Kishawy H A (2013) Prediction of cutting forces in broaching operation. J MANUF SYST 12(1): 1-14.

[10] Meng Z, Wu C, Ni J et al (2017) Modeling and analysis of cutting force in vibration-assisted broaching (VAB). INT J ADV MANUF TECH 91(5-8): 2151–2159.

[11] Seimann M, Peng B, Fischersworringbunk A et al (2018) Model-based analysis in finish broaching of inconel 718. INT J ADV MANUF TECH 97: 3751-3760.

[12] Hosseini A, Kishawy H A, Moetakefimani B (2016) Effects of Broaching Operations on the Integrity of Machined Surface. Procedia CIRP 163-166.

[13] Klocke F, Gierlings S, Adams O et al (2015) New Concepts of Force Measurement Systems for Specific Machining Processes in Aeronautic Industry. CIRP J MANUF SCI TEC 9(1): 31-38.

[14] Boud F, Gindy N (2008) Application of multi-sensor signals for monitoring tool/workpiece condition in broaching. INT J COMPUT INTEG M 21(6): 715-729.

[15] Axinte D, Gindy N (2003) Tool condition monitoring in broaching. WEAR 254: 370-382.

[16] König W, Klocke F (2011) Manufacturing processes. Springer, Berlin Heidelberg.

[17] Chatti S, Laperrière L, Reinhart G et al (2019) CIRP Encyclopedia of Production Engineering. Spring , Berlin.

[18] Merchant M E (1945) Mechanics of the metal cutting process. I. orthogonal cutting and a type 2 chip. J APPL PHYS 16(5): 318-324.

[19] Zhou L, Wang Z, Wen H (2019) On the Accuracy of the Johnson-Cook Constitutive Model for Metals. CHIN J HIGH PRESSURE PHYS 33(04): 3-16.

[20] Shi D, Axinte D A, Gindy N (2006) Online machining process monitoring using wavelet transform and SPC. Instrumentation and Measurement Technology Conference 2081-2086.

[21] Daubechies I (1992) Ten Lectures on Wavelets. Springer-Verlag, Berlin.

[22] Mallat S G (1998) A Wavelet Tour Of Signal Processing. Academic Press ,Amsterdam.